

Cite this: *Mater. Adv.*, 2022,
3, 6208

Robust and high barrier thermoplastic starch – PLA blend films using starch-*graft*-poly(lactic acid) as a compatibilizer†

Binh M. Trinh, Debela T. Tadele  and Tizazu H. Mekonnen *

This work reports the design of a single-layer robust and good barrier sustainable films by using graft polymer compatibilizers. A starch-*graft*-poly(lactic acid) (St-PLA) copolymer was synthesized and its efficacy as a compatibilizer of thermoplastic starch (TPS)/PLA blends was studied in detail. The St-PLA copolymer is synthesized using a tin(II) 2-ethylhexanoate initiator, employing ring-opening surface graft polymerization. The microstructure and morphology development of the blends are studied using a polarized optical microscope (POM), scanning electron microscope (SEM), differential scanning calorimetry (DSC), and rheology investigations. Results indicate that the addition of the St-PLA at 2.5 wt% and 5 wt% in the TPS/PLA blend via a melt extrusion process has tremendously improved the compatibility of TPS/PLA blends. Moreover, the PLA crystal spherulite size demonstrates considerable reduction with the addition of the St-PLA compatibilizer despite maintaining similar melt processing parameters. As a result of the improvement in microstructure and morphology changes, the compatibilized blends exhibit outstanding oxygen barrier and thermomechanical properties. Thus, the compatibilization effects provided by St-PLA offer a non-reactive approach to improve the overall morphology and physical properties of the immiscible TPS–PLA blends. Such blend can be used as a single layer flexible packaging material and allows repeated recycling.

Received 3rd May 2022,
Accepted 23rd June 2022

DOI: 10.1039/d2ma00501h

rsc.li/materials-advances

1. Introduction

The growing movement to impose strict environmental regulations on single-use plastics has accelerated innovation interest in sustainable materials as replacement for polyolefins and other traditional plastics.¹ The use of natural macromolecules to design biodegradable or compostable plastics offers potential solutions to concerns associated with the production and end-of life of synthetic plastics.^{2–4} Among the various sustainable polymers, poly(lactic acid) (PLA), poly(butylene succinate) (PBS), and poly(hydroxyalkanoate) (PHA), thermoplastic starch (TPS) attracted considerable interest. Other synthetic biodegradable polymers, such as poly(butylene adipate-*co*-terephthalate) (PBAT), poly(ϵ -caprolactone) (PCL), and poly(glycolic acid) (PGA), have also been extensively investigated as sustainable polymer alternatives.^{4,5}

PLA is perhaps the most investigated and utilized bio-based and compostable bioplastic produced from renewable

resources, such as corn, sugarcane, bagasse, *etc.* It is appealing due to its ease of processability using conventional processing techniques, thermal stability, good mechanical properties, excellent moisture barrier properties, and acceptable cost structure.⁶ However, the extensive utilization of PLA to displace polyolefins in packaging and engineering applications is still limited due to its high brittleness, poor oxygen barrier properties, and high cost compared to conventional polyolefin-based plastics.^{7,8} To enhance the gas barrier, conductivity, thermal, and physic-mechanical properties of immiscible blends, the incorporation of bio-based fillers such as modified nanoclays and carbon black particles have been employed as alternate solutions to improve thermoplastic composites as packaging materials.^{9,10} Another commonly used method is to combine PLA with other biopolymers that can complement PLA's weakness. For instance, thermoplastic starch (TPS) is an excellent candidate to complement the limitations of PLA in packaging and other applications of commercial interest owing to its inherent attributes of biodegradability, abundance, high oxygen barrier properties and most importantly, cost-structure.^{11–13} Furthermore, many studies have found that a blend of TPS and PLA has the potential to bring a balance in the desirable complementary properties between both materials. Polymer blends can either be miscible or immiscible, in which the

Department of Chemical Engineering, Institute of Polymer Research, Waterloo
Institute of Nanotechnology, University of Waterloo, Waterloo, ON, Canada.
E-mail: tmekonnen@uwaterloo.ca

† Electronic supplementary information (ESI) available. See DOI: <https://doi.org/10.1039/d2ma00501h>



miscibility of polymer blends refers to a homogenous morphology with a negative Gibbs free energy of mixing.¹⁴ Binary blends of TPS and PLA are immiscible due to the poor interfacial tension and phase adhesion and rheology factors, which results in poor microstructure development. Thus, producing a stable immiscible blend and controlling the microstructure of TPS and PLA remained a remarkably challenging task. In addition to process optimization, the use of additives, such as compatibilization agents can mitigate such challenges.

Compatibilizers for immiscible blends can be classified into two main categories: (1) *in situ*: reactive compatibilizers containing reactive functional groups (maleic anhydride, epoxy, *etc.*) that can interconnect different polymer phases by generating chemical bonds between functional groups (hydroxyl, carboxyl, *etc.*) of the polymer chains; (2) *ex situ*: non-reactive compatibilizers (typically premade copolymer) that are miscible to all constituents in the blends.^{15,16}

Several studies have reported the improvement in the mechanical properties of PLA/TPS blends by increasing the interfacial adhesion *via* utilizing various *in situ* compatibilizers, with various degrees of success.^{7,17–20} Huneault *et al.* successfully prepared PLA/TPS blends using maleic anhydride compatibilizer, resulting in a considerably ductile blend over the uncompatibilized alternative.¹⁷ Another study by Turco *et al.*, demonstrated biodegradable films of PLA thermoplastic corn starch blend using epoxidized oil as an *in situ* compatibilizer.¹⁹ While the interfacial adhesion between the hydrophobic PLA and hydrophilic TPS improved as a result of the epoxidized oil, phase separation between the PLA and TPS resumed with secondary processes. As a result, the compatibilization did not enhance mechanical properties. Shi *et al.* utilized a different *in situ* approach of synthesizing glycidyl methacrylate grafted poly(ethylene octane) (GPOE) to be used as the third component of a PLA/TPS/GPOE ternary blend, which showed significant improvement in mechanical morphology, water absorption, and degradation properties.²⁰

On the other hand, the utilization of *ex situ* starch-graft-copolymer in immiscible TPS/PLA blend has been previously proposed, the information obtained is still limited. Recently, there have been numerous attempts to attach PLA chains onto anhydroglucose units (AGU) (*e.g.*, starch, nanocellulose, carboxymethyl cellulose) by utilizing “grafting from” technique to grow the oligomer chains from lactic acid (LA) or L-lactide and generate graft copolymers.^{21–24} It is believed that, in theory, the PLA block from the graft copolymer can be miscible to the PLA phase, while the starch block can be miscible to the TPS phase in the blend. Thus, making the graft copolymer Starch-graft-PLA (St-PLA) an interesting and viable option to improve the miscibility of TPS/PLA blend. To the best of our knowledge, investigation on the effects of *ex situ* St-PLA compatibilizer on the overall morphology, crystallinity, and barrier properties of TPS/PLA blend has not been explored in previous research. Thus, this work offers an in-depth investigation on the chemical characterization of the *ex situ* compatibilizer St-PLA synthesized through the ring open polymerization (ROP) reaction and carries out a comprehensive study on the interaction

between TPS and PLA polymer chains bridged together by the *ex situ* compatibilizer St-PLA. The compatibilized blend's morphology, rheology, crystallinity, and physical properties as the results of incorporating the compatibilizer were also reported.

2. Methods and materials

2.1. Materials

Corn starch (containing approximately 73% amylopectin and 27% amylose) was supplied by Sigma Aldrich, USA. Polylactide (PLA) resin ($\rho = 1.24 \text{ g cm}^{-3}$, $M_w = 168\,000 \text{ g mol}^{-1}$) in pellet form (Ingeo™ biopolymer 4043D general grade) was obtained from Nature Works LLC, Minnetonka, MN, USA. L-Lactide monomer was purchased from TCI America. Other chemicals such as tin(II) 2-ethylhexanoate (Sn (Oct)_2), potassium bromide (KBr) in powder form, sodium hydroxide (NaOH) pellets, 10.2 N hydrochloric acid (HCl), dimethyl sulfoxide (DMSO) (99.9%), deuterated DMSO (DMSO-d_6), methanol (MeOH), ethanol (EtOH) (99.0%), and rubbing alcohol (2-propanol) (99.0%), were all purchased from Sigma Aldrich, USA. All chemicals were used as received.

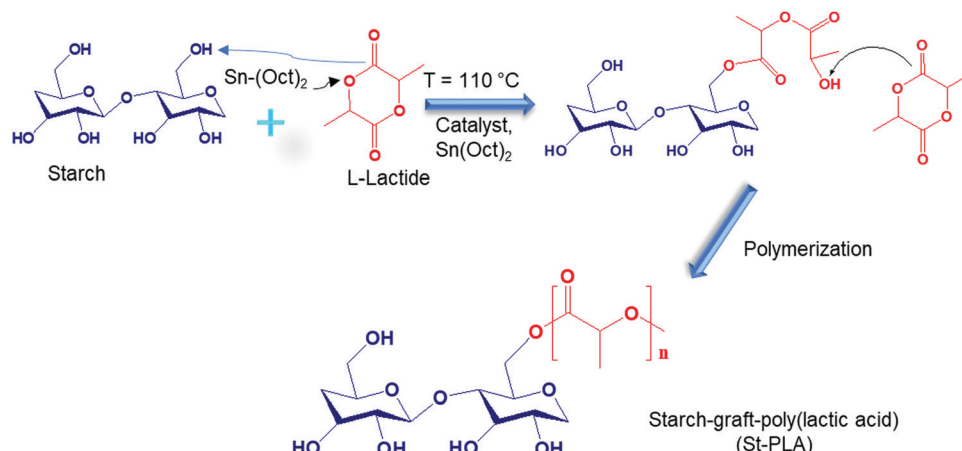
2.2. Methods

2.2.1. Grafting of PLA onto starch chains. The preparation of poly(lactic) grafted starch for characterization was carried out using L-lactide as a monomer for the ring-open polymerization process, as illustrated in Scheme 1. 10 wt% of corn starch powder was solubilized in DMSO at 90 °C in a round bottom flask reactor and immersed in silicon oil that was placed on a magnetic stir plate. 8 vol% of the Sn (Oct)_2 catalyst was then added to the solution. Specific ratios of the solid L-lactide (Table 1) with respect to the starch were then slowly added to the mixture over 5 min and constantly agitated (250 rpm). The reaction was allowed to run for 24 h at 110 °C. The modified product (referred to as St-PLA) was recovered *via* isopropanol precipitation followed by ethanol washing (three times) and methanol washing (three times) to remove unreacted lactide and excess Sn (Oct)_2 . Complete removal of the excess Sn (Oct)_2 was confirmed by infrared analysis of raffinate from the last washing step. The washed solid sample was subsequently dried at 70 °C overnight, ground into a fine powder, and stored in a glass vial at room temperature for further analysis.

2.2.2. Characterization of the modified CNCs

Fourier transform infrared spectroscopy (FTIR). The grafting of PLA chains onto corn starch particles was characterized at ambient temperature using FTIR (Nicolett 6700, Thermo Scientific Inc.). Native and modified starch samples for the IR were prepared by mixing the powder samples with KBr salt (2 mg sample and 200 mg KBr) and pressing them into pellets. On the other hand, PLA was prepared by adding the PLA in chloroform solvent directly to a potassium bromide (KBr) salt pellet and dried under vacuum overnight. FTIR scans, in transmittance mode, were recorded in the range of 4000 to 500 cm^{-1} under the same conditions as the background.





Scheme 1 Ring open polymerization reaction to synthesize Starch-graft-PLA (St-PLA) copolymer.

Table 1 Concentration of material used to produce St-PLA

Copolymer (compatibilizer)	Starch (g)	Lactide (g)
St-PLA 1	10	2.5
St-PLA 2	10	5
St-PLA 3	10	10

Proton nuclear magnetic resonance (H-NMR). Proton nuclear magnetic resonance (H-NMR) spectra of the baseline and grafted starch (St-PLA) at different modification levels were recorded to analyze the chemical changes resulting from the reaction. For this, the samples were dissolved in deuterated dimethyl sulfoxide (DMSO- d_6) at 50 °C and sealed in 5 mm NMR analysis tubes with a ratio of 10 mg solid sample to 0.7 mL solvent. The H-NMR spectra were collected from 0 to 7 ppm using Bruker 500 MHz high-resolution NMR (Bruker-SpectroSpin 500 MHz Ultra shield, Bruker Corporation, MA).

Thermogravimetric analysis (TGA). The impact of PLA grafting on the thermal degradation behaviour of starch was evaluated by conducting TGA on pristine and modified samples. The tests were carried out on dried samples using TA instrument TGA Q500. The test was carried out from 30 to 500 °C at 10 °C min⁻¹ heating rate and a nitrogen flow of 20 mL min⁻¹.

Differential scanning calorimetry (DSC). The thermal transitions profiles of starch, TPS, PLA, and TPS/PLA (non-compatible and compatibilized) blends were analyzed using DSC (Q2000, TA instrument, USA). For the test, accurately weighted samples of 5 mg were placed in a sealed aluminum pan, and the test was run in a nitrogen atmosphere of 50 mL min⁻¹. An empty aluminum pan was used as a reference for all scanning measurements. The thermal profiles were obtained from 10 to 190 °C with the ramping rate of 10 °C min⁻¹. For the blend film samples, specimens were first scanned from 20 to 200 °C at a ramping rate of 10 °C min⁻¹ to remove the thermal profile. Next, the samples were kept at 200 °C for 5 minutes, cooled down to -75 °C at cooling rate of 10 °C min⁻¹, and heating up again from -80 to 200 °C at the ramping rate of

10 °C min⁻¹. The percentage crystallinity of PLA phases within the blend was determined using eqn (1).

$$\chi_c(\%) = \left(\frac{\Delta H_m - \Delta H_{cc}}{\Delta H_m^0} \right) \times 100\% \quad (1)$$

where ΔH_m and ΔH_{cc} are the melting and cold crystallization enthalpy of the PLA in the sample blends, respectively. ΔH_m^0 is the melting enthalpy of the theoretical 100% crystallized versions ($H_m^0 = 93.7 \text{ J g}^{-1}$).²⁵

Water contact angle (WCA). Using a custom-built optical sessile drop system, the water contact angle (WCA) measurement of starch and St-PLAs was carried out. About 5 μL of the water droplet was dropped onto the prepared pellets, and images were taken after 10 seconds. A built-in Matlab tool was used to measure the contact angles of the water droplets.

2.2.3. Preparation of TPS. Corn starch was dried at 70 °C overnight to obtain a moisture level below 1%. Glycerol at 30% w/w concentration with respect to the corn starch mass was added, mixed evenly, and left inside a sealed container for 24 h before processing. The prepared mixture was then fed into a twin-screw extruder (Process 11 Parallel Twin-Screw Extruder, Thermo Fisher Scientific) with a barrel diameter of 11 mm and L/D ratio of 40. The temperature profile used for extrusion was 110/115/115/120/120/120/125/125 °C from the feed throat to the die exit, and the screw speed was set at 150 rpm. The extruded samples were air chilled, pelletized and stored in an airtight container. The density and molecular weight (M_w) of the extruded TPS was experimentally determined to be approximately 1.09 g cm⁻³ and 35 000 g mol⁻¹, respectively.

2.2.4. Preparation of the ex situ compatibilized TPS/PLA immiscible blends. After selecting the optimal starch grafted PLA (St-PLA), the designated modified starch was incorporated into the TPS/PLA blend formulation at various concentrations listed in Table 2. The St-PLA demonstrates good dispersion in water using a rotor-stator homogenizer (Homogenizer, Power-Gen 700). A blend of TPS/PLA (ratio 60/40) was mixed well together with the water dispersed compatibilizer St-PLA, dried at 80 °C for 48 h and equilibrated in an air-sealed container for



Table 2 Formulations of TPS/PLA blends and their compatibilized counterparts

Sample	Blend compositions		Compatibilizer
	TPS (%)	PLA (%)	St-PLA2 (%)
TPS	100	0	—
TPS/PLA	70	30	—
TPS/PLA/1%St-PLA	70	30	1
TPS/PLA/2.5%St-PLA	70	30	2.5
TPS/PLA/5%St-PLA	70	30	5
PLA	0	100	—

at least 24 h. The blend was then fed into the twin-screw extruder (Process 11 Parallel Twin-Screw Extruder, Thermo Fisher Scientific) with temperature profile of 160/170/175/180/180/180/185/185 °C from the feed throat to the exit die, and screw speed of 100 rpm. The blended samples were air chilled, pelletized, and stored in zip-lock bags.

2.2.5. Fabrication of TPS/PLA film. To fabricate the films from the blend composition, extrusion processed pellets were first dried in an oven (70 °C for 24 h) to remove residual moisture. A measured quantity of the dried blends was then melt-pressed into thin 10 × 10 mm bioplastic film *via* compression molding (Carver press, IN, USA) using a 0.15 mm mold spacer for 5 min at a temperature and pressure of 180 °C and 5000 psi, respectively.

2.2.6. Characterization of the films

Scanning electron microscopy. The fractured surface morphologies of neat and compatibilized blend films were investigated using FEI SEM (Quanta FEG-SEM 250, Oxford Instrument) at an accelerating voltage of 20 kV. The fractured surfaces were coated with gold sputtering and mounted onto stubs with double-sided carbon adhesive tape prior to scanning.

To further determine the phase morphologies of the immiscible blend, phase-extracted samples were prepared. The cryo-fractured samples of each blended formulation was immersed in 10.2 N HCl solution at 25 ± 2 °C for 8 h to remove the TPS phase. The TPS leached specimens were then rinsed with water and ethanol and dried at 70 °C for 48 h.

Polarizing optical microscope (POM). A polarizing optical microscope (Olympus BX53M polarizing optical microscope, USA) was employed to determine the crystal morphologies of TPS-PLA blends with and without the co-grafted-compatibilizer St-PLA. Pictures were collected at 20× objective magnifications.

Rheometer. Rheology measurements, such as the complex viscosity, elastic modulus (G'), and viscous modulus (G'') of the various emulsion formulations were studied at 180 °C using a stress-controlled rotational rheometer (HAAKE Mars 3, Thermo Scientific) with a parallel plate geometry and a gap of 1 mm between the plates. Rheology samples with diameters and thicknesses of 15 and 3 mm, respectively, were used for the measurement.

UV-Vis. The light transmittance of the samples was recorded using Cary 100 Bio UV-Vis's spectrophotometer at the visible wavelength of 600 nm to determine the transparency of the

films. Opacity values were calculated by converting the transmittance at wavelength 600 nm to absorbance and dividing by the films' thickness.

Barrier properties. The water vapor permeability of the film formulations was evaluated in accordance with ASTM E96/E96M-16. The water vapor transmission rates (WVT) were measured using barrier cups with an exposed area of 10 cm². The barrier cups were filled with 7 mL distilled water (RH = 100%) with the film placed over the opening of the cups and tightly clamped with screw lids. The cups were then placed inside a sealed chamber at 23 °C and 30% relative humidity. The weight loss resulting from water permeation through the film was recorded at different time intervals up to seven days. WVT values (g m⁻² h⁻¹) were then determined using eqn (2):

$$\text{WVT} = \frac{\Delta G}{t} \times \frac{1}{A} \quad (2)$$

where $\Delta G/t$ (g h⁻¹) is the linear slope of the weight loss *vs.* time graph, and A (m²) was the exposed area of the water barrier cup. WVP values (kg m m⁻² s⁻¹ Pa⁻¹), was calculated based on eqn (3):

$$\text{WVP} = \frac{\text{WVT} \times l}{S(\text{RH}_1 - \text{RH}_2)} \quad (3)$$

where l (m) was the thickness of the films; S was the saturation vapor pressure at 23 °C; RH_1 and RH_2 were the fractional relative humidity in the inside and outside of the test cup, respectively. Three specimens for each sample were used, and the average values were reported.

The oxygen permeability (OP) tests were performed using a customized bubble flow rate setup. Films (18.10 cm²) were used to seal a two-chamber cartridge attached to an oxygen gas source on one end and a bubble flow meter on the other end. The pressure difference between the two chambers was set at 5 psi, allowing the oxygen to permeate through the membrane. The flux of bubbles was determined by counting the time the bubbles took to travel 50 mL volumetric unit. The OP values (cm³ m m⁻² day⁻¹ Pa⁻¹) was then calculated using eqn (4):

$$\text{OP} = \left(\frac{V}{t \cdot A} \right) \times \frac{l}{\Delta P} \quad (4)$$

where $V/(t \cdot A)$ (cc m⁻² day⁻¹) is the flux of oxygen; l (m) was the thickness of the films; and ΔP (Pa) is the pressure difference between two sides of the film. Triplicate measurements were conducted at room temperature 23 °C and 30% RH.

Tensile property testing. Tensile property testing was carried out using a Universal tensile testing unit (AGS-X series, Shimadzu, Japan) with a 500 N load cell according to ASTM D882-18. Films were cut into 70 × 10 mm test pieces with a gauge length of 50 mm. The sample's thickness was collected by taking the average values of 3 measurement points across each sample. Testing was conducted at room temperature and 5 mm min⁻¹ strain rate. At least five samples were tested for each formulation, and the average was reported.



2.2.7. Statistical analysis. Data in this work is presented as mean \pm standard deviation. Statistical differences in data were determined using one-way analysis of variance (ANOVA). A significance level of $\alpha < 0.05$ was employed.

3. Results and discussions

3.1. Characterization of starch-graft-PLA copolymer

FTIR. The presence of a PLA chain grafted onto starch granules was confirmed through IR analysis. A comparison of the spectra between starch and PLA grafted starch (St-PLA) with various lactide concentrations is presented in Fig. 1. As anticipated, starch displays characteristic signals of AGUs, including a broad spectral band of OH ($3600\text{--}3000\text{ cm}^{-1}$), C–H stretching ($2930\text{--}2850\text{ cm}^{-1}$), peaks at $1200\text{--}980\text{ cm}^{-1}$ (C–O stretching, C–C stretching, and C–O–H bending), and 950 cm^{-1} (α -glycosidic linkages), which were reported in other literature.^{23,26,27} The graft-co-polymerized St-PLA exhibited a new sharp peak at 1739 cm^{-1} , which grew in intensity with increasing the concentration of lactide in the reaction. The appearance of this new peak corresponds to the stretching of the ester carbonyl bond (C=O) attributed to the grafting of PLA oligomers onto starch, as illustrated in Scheme 1. Other studies on the synthesis of PLA grafts reported the emergence of a similar peak.^{24,28} Another evidence for the grafting of lactic acid oligomer on starch was the progressive reduction of the broad hydroxyl vibration at $3600\text{--}3000\text{ cm}^{-1}$, indicating that (–OH) group was substituted. The stretching of PLA's –CH could overlap with starch's strong –CH stretching at 2930 cm^{-1} . Peaks at 1650 cm^{-1} , assigned to absorbed water molecules on starch's structure, reduced with the increase in the grafting of PLA, which could be associated with an increase in hydrophobicity. Overall, the results obtained from IR spectra indicate that the lactide was successfully grafted and polymerized into PLA oligomers on the anhydroglucose units of starch through ROP reaction with Sn (Oct)₂ as the catalyst initiator.

H-NMR results. The grafting copolymerization of L-lactide onto starch to create St-PLA was further validated using H-NMR spectra (Fig. 2) through the identification of new hydrogen

peaks associated with chemical structure change. The strong peak at 2.50 ppm was associated with deuterated DMSO (DMSO-d₆) solvent that used to dissolve the pristine and modified starch samples. Moreover, the pristine and the St-PLA spectra exhibited characteristic peaks of anhydroglucose units (AGU) in the 5.70–3.00 ppm region. These signature anhydroglucose peaks were identified at 5.60–5.54 ppm (O–H protons at positions 2 and 3), 4.45 ppm (O–H protons at position 6), 3.60 ppm (protons at positions 3/5/6/6'/6''), and 3.30 ppm (protons at positions 2/4/).^{6,29,30} The NMR peaks at 5.20–5.10 ppm represent the proton on the linear α -1,4 linkages (position 1 and 1') and branching α -1,6 linkages (position 1') of starch, respectively.^{29,31,32}

The NMR signals of commercial-grade PLA was also examined for comparison purpose. The PLA sample was dissolved in deuterated chloroform (CDCl₃), which correspond to the NMR peak at 7.2 ppm, as shown on the PLA spectrum in Fig. 2. Furthermore, the PLA displayed two distinctive peaks at approximately 5.2 and 1.5 ppm, which correspond to the hydrogen atoms attached at the carbon backbone (position a) and the methyl group –CH₃ (position b), respectively.^{33,34}

The spectra of the synthesized St-PLA revealed additional signals that correspond to the grafted PLA oligomer, as well as the lactic acid monomer, on the AGUs. The emergence of an additional signal at approximately 1.5 ppm that was not observed in starch, and the overlapping signal intensity at about 5.2 ppm, were emanating from the grafted PLA oligomer on the AGU of starch. Similar peaks were also observed in the PLA spectra, implying that the PLA chains were successfully synthesized and grafted on the starch structure. Also, it is noteworthy to mention the gradual increase in the intensity and eventually overlapping of peaks at 5.20 ppm with the increase in L-lactide concentration, indicating the ring opening polymerization of PLA oligomers. The degree of substitutions (DS) of OH with the modifying agent can usually be determined *via* integrating anomeric proton peaks at 5.20 ppm and the hydroxyl protons from PLA oligomer chain end at 4.40–4.00 ppm. However, the DS for St-PLA sample was not feasible due to the interference of the overlapping peaks at 5.2 ppm. The presence of new peaks at around 4.4–4.2 ppm, as well as a peak at 1.3 ppm attributed to the protons at position c, were detected for only the St-PLA samples. It is suspected that since the synthesized PLA on the AGU unit has much shorter chain lengths compared to commercial PLA, the peaks at 1.3 ppm were potent in St-PLA samples while completely missing in the commercial PLA spectra. A similar observation was reported by Noivoil and Yoksan,³⁵ in which they reported a similar peak at 1.3 ppm position corresponding to the methyl group proton at the PLA chains end. Thus, it was determined that the grafted PLA chains were oligomers instead of fully grown polymer chains. On the other hand, the emergence of a peak at 4.4–4.2 ppm, could plausibly correspond to the proton signal of O–H at position d. Thus, the NMR results confirmed the lactic acid grafting and subsequent polymerization onto the starch chain.

Thermal analysis of St-PLA. Thermal degradation analysis was carried out to investigate the changes in thermal stability of

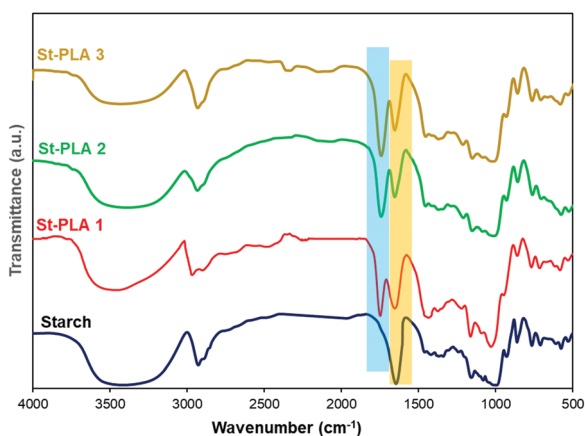


Fig. 1 FTIR spectra of neat starch and graft copolymer St-PLA.



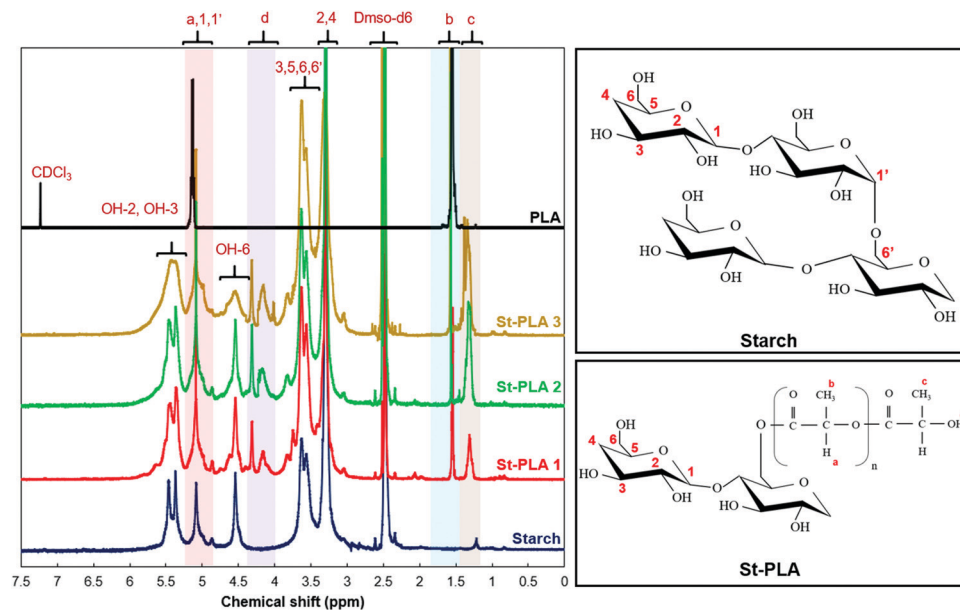


Fig. 2 H-NMR spectra of neat starch and graft copolymer St-PLA at different grafting level.

the modified starch as a result of the graft polymerization. The thermogravimetric analysis (TGA) and derivative (DTG) curves are presented in Fig. 3(a) and (b), respectively. Native corn starch exhibited typical thermal decomposition peaks around 310 °C and left a residue of approximately 20 wt%, which correspond to the charring of AGU ring. This observation agrees with previous studies on thermal analysis of polysaccharides. However, the thermogram of the modified St-PLA samples displayed gradually reducing onset degradation temperatures with increasing concentration of lactide in the reaction, with the St-PLA3 displaying the lowest degradation temperature at 270 °C. As expected, the DTG peaks of the modified samples diminished as the concentration of lactide increased, suggesting that the ROP modification significantly reduced the packed crystalline structure of the native starch. Thus, replacing the (–OH) group with PLA oligomers effectively hinders the inter and intramolecular hydrogen bonding of starch, which lowers the thermal stability of the compatibilizer. It was also interesting to observe the appearance of an additional small degradation peak at around 450 °C across all the three modified samples, which was likely attributed to the degradation of the grafted PLA oligomers.

The thermal profiles of St-PLA samples were further evaluated *via* DSC, and results are shown in Fig. 3(c). The DSC of the pristine starch presented a smooth line with no peaks, indicating the absence of transition phase (cold crystallization, melting point) in the thermal run. On the contrary, all the St-PLA samples exhibited an endothermic peak at around 150 °C, attributed to the melting of the PLA oligomers grafted onto starch. One notable observation was the lack of cold crystallization peaks in the St-PLA profiles. Based on their work on the grafting of PLLA onto starch Chen *et al.*, suggested that the crystallization behaviours of the starch-PLLA depend on the PLLA length.²¹ Thus, in line with the NMR observation,

the grafted PLA chains in this study did not produce many long-chain PLA, which explains the missing cold crystallization peaks expected in the St-PLA samples. Overall, the results from DSC indicated that PLA oligomers were successfully synthesized on the surface of the starch. However, the chains are short, which was demonstrated by the thermogram's lack of cold crystallization peaks.

Water contact angle. Water contact angle (WCA) measurement is a well-established method to investigate the surface polarity of polymers. The water contact angle values for starch and St-PLA oligomers (Fig. 3(d)) had an increasing trend with an increase in the level of grafted PLA. As anticipated, starch samples exhibited the lowest contact angle (17°), indicating the polarity attributed to the abundant –OH groups on the structure. On the contrary, the St-PLA samples displayed a larger contact angle that increased with the increase in the level of PLA grafting. In the two most modified samples, the water contact angle improved up to 36 and 41° for St-PLA 2 and St-PLA 3 samples, respectively, which validated the ROP reaction replacing the –OH groups with PLA oligomers. It was interesting to observe that although the WCA increases, the modified samples are still hydrophilic as the WCAs were still <90°. This behaviour has emanated from the lack of fully grown PLA chains on the surface of the starch. Based on the results obtained from thermal analysis and WCA, the modified St-PLA2 showed appealing characteristics as it exhibited balanced thermal stability and surface polarity levels. Thus, St-PLA2 was selected as the representative *ex situ* compatibilizer for the TPS–PLA blend film fabrication.

3.2. Compatibilized blends of TPS–PLA

Morphology of blends. SEM was employed to examine the morphology of fractured sample surfaces (Fig. 4). As expected, both the TPS and PLA single phases displayed smooth fracture



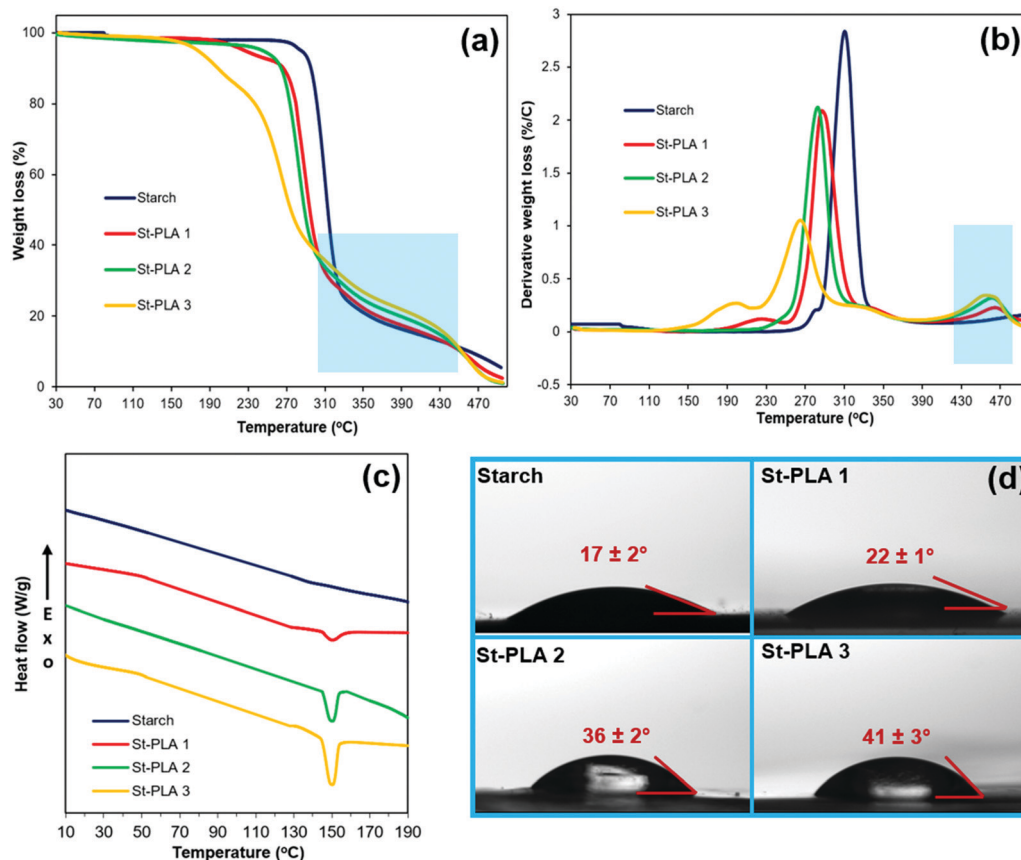


Fig. 3 (a) TGA spectra, (b) DTGA spectra, (c) DSC spectra, and (d) WCA of starch and St-PLA at different grafting level.

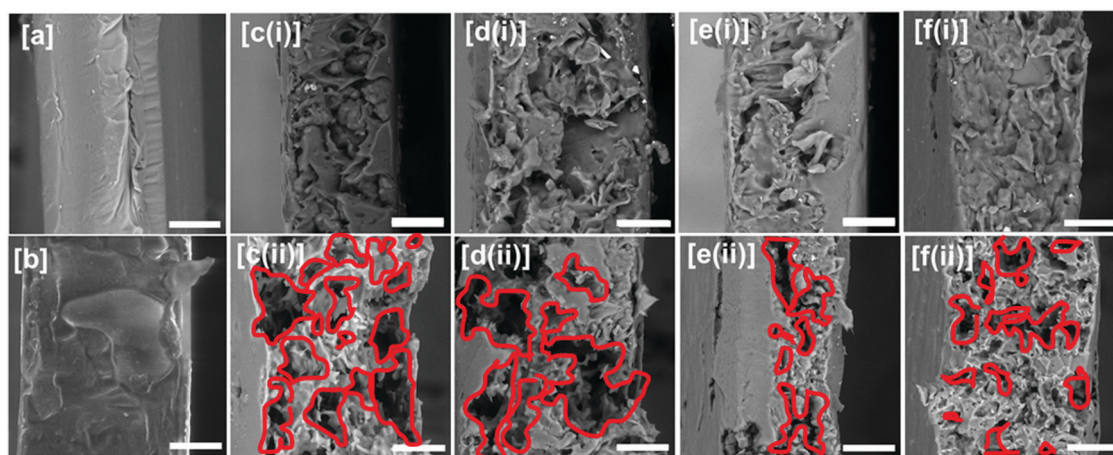


Fig. 4 SEM images of (a) neat TPS, (b) neat PLA, (c) TPS/PLA, (d) TPS/PLA/1% St-PLA, (e) TPS/PLA/2.5% St-PLA, and (f) TPS/PLA/5% St-PLA. (i) is for normal cross-sectional fracture of sample films, (ii) is for the sample films etched with HCl to remove TPS phase. The white bars represent 20 μm.

surfaces. On the contrary, the uncompatibilized TPS/PLA blend demonstrated rough fracture surfaces, phase separation, and voids, suggesting the lack of compatibility between the two polymers. Nonetheless, the addition of the *ex situ* compatibilizer St-PLA has visibly smoothed the fractured surface and reduced the voids in the blend, suggesting greater blend

homogeneity between the polymers. The increased cohesiveness and smoothness owing to the effect of compatibilization was observed to improve as the concentration of St-PLA increased. This was because the St-PLA can interconnect and bind the phases of PLLA and starch granules. To gain a better understanding of the phase dispersion, distribution, and



compatibility of the blend components, the cryofractured blend samples were subjected to concentrated HCl etching to remove the TPS phase. The etched samples were then examined using SEM (Fig. 4(c)–(f)–(ii)). The non-compatible blends were noticeably devoid of the TPS phase (red islands), indicating that the continuous phase was TPS while the dispersed phase was attributed to PLA in the matrix-droplet model. When St-PLA was incorporated in the blends, the amount of TPS removed seems to decrease, indicating that the PLA was partially miscible or bound to the TPS limiting TPS leaching by the solvent etching. With the use of 2.5 and 5 wt% St-PLA (Fig. 4(e), (f)–(ii)), the retainment of TPS was more evident, indicating the good interfacial miscibility and bonding between the TPS and PLA phases. Overall, increasing the concentration of St-PLA compatibilizer can lead to better enhancement of interfacial compatibility and potentially improve the overall morphology of the immiscible TPS/PLA blend.

Crystallization investigation via POM and DSC. The crystal morphology structure of TPS/PLA blends with the addition of the co-graft-polymerized St-PLA compatibilizers was further evaluated with POM equipped with a polarizer (Fig. 5(a)). The spherulite petals observed in TPS/PLA blends were contributed mainly by the PLA phase in the immiscible blend. This characteristic structure of spherulites has been observed and reported in other studies on the crystallinity of PLA. Compared to those presented in neat TPS/PLA blends, the PLA spherulites observed in the formulation containing St-PLA were smaller and dispersed, indicating that the PLA phases in the compatibilized blends are distributed more evenly. As depicted in Fig. 5(a), the numbers of observed PLA spherulites have considerably reduced at the highest St-PLA loading of 5 wt%. Additionally, there is a slight reduction in the spherulite sizes when the compatibilizers were added. It is plausible that the presence of the St-PLA compatibilizers could plasticize and interfere with the PLA chains in the inclusion phase between the TPS and PLA interfaces, which ultimately reduced the overall crystalline spherulite structure of PLA phases during melt extrusion resulting in enhanced interfacial interaction between the blend components. By increasing the

concentration of St-PLA compatibilizers, the reduction in crystallinity became more apparent and resulted in a massive drop in the number of spherulites observed in the immiscible blend.

The crystalline structure of the TPS/PLA blends was further evaluated by monitoring the change in the thermal transitions provided by DSC. A summary of the various transition temperatures during the second heating, such as glass transition temperature (T_g), cold crystallization temperature (T_{cc}), melting temperature (T_m), cold crystallization enthalpy, melting enthalpy, and crystallinity are presented in Fig. 5(b) and Table S1 (ESI[†]). It was noted that the TPS behaved more like an amorphous material and did not exhibit any measurable thermal transition from the DSC. On the other hand, PLA displayed clear T_g , T_{cc} , and T_m , with a low crystallinity level (10.3%), indicating its semicrystalline behavior. It was interesting to observe that the TPS/PLA blend without compatibilizer exhibit only one melting peak (at 145 °C) similar to PLA's thermogram, while all the blends containing St-PLA exhibit two distinctive peaks. This was attributed to the two melting peaks of TPS/PLA corresponding to the two distinguished behaviours of PLA chains in the blend. The first peak around 140–143 °C was attributed to PLA entangled with TPS chains due to the enhanced interaction caused by the St-PLA. This crystalline structure would melt faster due to the ease of the chain segments to move to a lower energy level. A similar observation was reported by Zhang *et al.* on the reactive blend of PLA with natural rubber, in which the authors have observed two distinctive peaks in their compatible blend.³⁶ Since the uncompatibilized TPS/PLA blend lacks compatibility, the lower temperature DSC thermogram was not observed. On the contrary, the second peak at 149–151 °C corresponds to the crystalline melting of PLA chains, similar to the existing peaks in PLA and TPS/PLA samples.

As shown in Table S1 (ESI[†]), the crystallinity has gradually reduced with the increasing concentration of St-PLA incorporated into the formulations. At 5 wt% St-PLA, the crystallinity of the blend has declined to only 1.86%. The observed reduction in crystallinity was in line with the POM imaging observations. Moreover, the reduction in crystallinity content within the

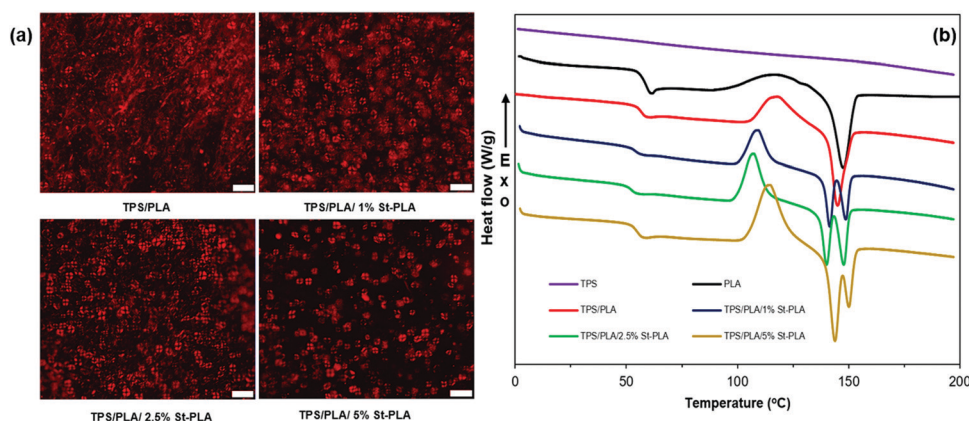


Fig. 5 (a) Microscope images and (b) DSC of non-compatible and compatibilized TPS/PLA blends.



polymers indicate a greater increase in the intensity of T_g (step height).³⁷ Similarly, the blends containing the St-PLA compatibilizer exhibited gradual enhancement in the region of T_{cc} transition. Most likely, these peaks intensification are attributed to the additional enthalpy required for the nuclei to form crystalline structures due to the addition of the St-PLA copolymer compatibilizers. The enhancement in step height and cold crystallization peaks are most evident in the TPS/PLA/5% St-PLA sample, showing that the crystallinity of the compatibilized blend has diminished. Thus, it was determined that the improved dispersion of PLA in the TPS continuous phase could reduce the PLA crystallization due to the St-PLA compatibilizer interference.

Rheology. The rheological properties of the TPS/PLA blends were evaluated using oscillatory shear flow at 180 °C to understand the effect of the St-PLA *ex situ* compatibilizer on the viscoelastic properties and processability of the blends. The storage modulus (G'), loss modulus (G''), and complex viscosity (η^*) as the functions of frequency were collected and presented in Fig. 6. In general, PLA displays a steep storage and loss moduli slope, while TPS/PLA blends show more plateau slopes due to the addition of the TPS phase. The introduction of the compatibilizer St-PLA in the blends results in reducing both the storage and loss moduli at low frequency. This was because the St-PLA compatibilizer promotes the bridging and entanglement of the TPS and PLA chains in the blend (Fig S1a–c, ESI†). Consequently, it helped the recovery of the deformation during shearing and hence reduced the storage modulus.

Moreover, since the shearing deformation of TPS chains was easier to recover, it would inherently dissipate less energy and reduce the loss modulus. This is because TPS chains are not as mobile as PLA with glycerol as a plasticizer. On the other hand, the overall moduli of all blends did not change regardless of the compatibilizer content at higher frequency.

Fig. 6(c) displays the complex viscosity of neat PLA and various TPS/PLA blends at 180 °C. PLA exhibited characteristic Newtonian behaviour with the viscoelastic plateau at a lower frequency, while TPS/PLA blends displayed non-Newtonian shear thinning behaviour in the entire frequency region. The observed shear-thinning behaviour of the TPS/PLA blends was attributed to the dominant viscosity of the continuous TPS

matrices due to forming a rigid three-dimensional starch network. Similar viscosity behaviour was noted in a recent investigation on the morphology–rheology relationship in coplasticized TPS/PLA blend.³⁸ The gradual decrease in the complex viscosity at lower frequency was observed with increasing incorporation of the St-PLA. As anticipated, the increased miscibility between the polymer chains of TPS and PLA due to interfacial bridging by St-PLA allows the chains to exhibit better movements at low frequency and reduce the overall intermolecular cohesive energy, which ultimately resulted in the complex viscosity reduction of the compatibilized samples. This reduction in complex viscosity trend can be correlated to diminishing in the crystalline structure of the blend. The drops in crystallites of TPS/PLA blend may break the ordered structures and facilitates mobility freedom for the branched PLA chains, which would lower the overall moduli and complex viscosity at lower shear rates. Overall, the dynamic rheology result gave crucial information on the compatibilization effect and processability of the TPS/PLA blend, which further supported the morphology observations.

Optical clarity. The transparency of plastics is one of the most desirable traits for a range of commercial materials, such as packaging films and coatings, and is dependent on the molecular microstructure and morphology of the constituent polymers. The light transmittance of the films fabricated from the control and blend samples was performed using Cary 100 Bio UV-Vis's spectrophotometer in the wavelength range of 350 to 800 nm to determine the transparency of the films. Opacity values were then calculated by converting the transmittance at wavelength 600 nm to absorbance and dividing by the films' thickness. The TPS and PLA, as individual films, exhibited excellent transparency (Fig. 7(a)). However, the opacity increased in the blends due to the poor compatibility of the TPS and PLA components (Fig. 7(a) and (b)). The addition of the St-PLA compatibilizer significantly improved the transparency of the films. According to Lin *et al.*, the bigger crystallites presented in semi-crystalline polymers can scatter light in a film, leading to poor transparency.³⁹ Thus, the addition of compatibilizers in this case may also play a part in decreasing in opacity (improved transparency) of the film. At the highest concentration of the St-PLA incorporation (5 wt%), the TPS/PLA

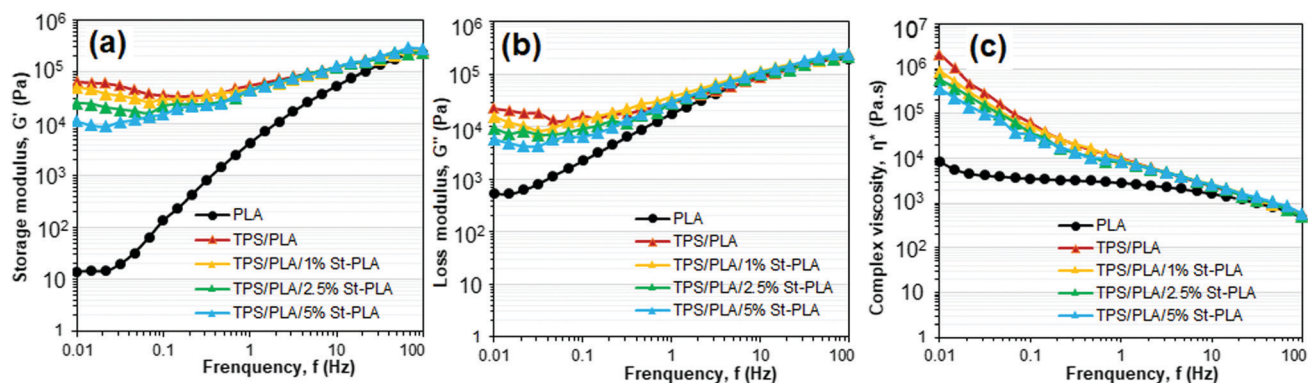


Fig. 6 Rheology showing (a) storage modulus, (b) loss modulus, (c) and complex viscosity as function of frequency of PLA and TPS/PLA blends.



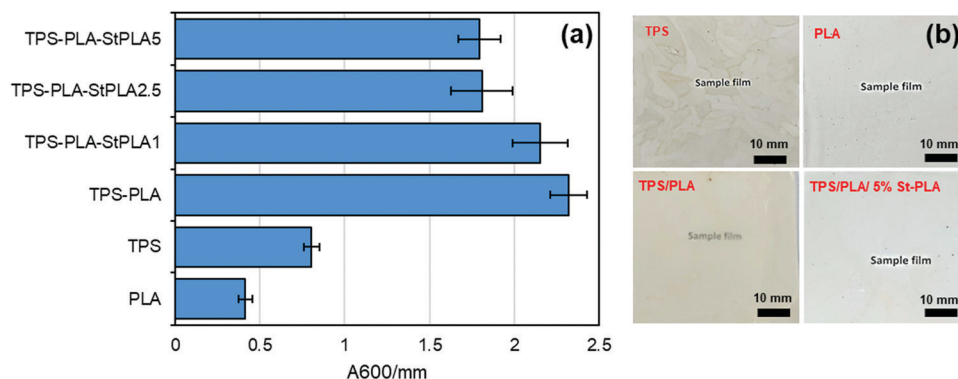


Fig. 7 (a) Opacity of films calculated as the ratio transmittance at 600 nm to the film thickness in mm ($A_{600} \text{ mm}^{-1}$), (b) Photographs of representative films.

blend demonstrated an opacity of $1.79 A_{600} \text{ mm}^{-1}$, which corresponds to 22.8% improvement compared to the non-compatibilized TPS/PLA blends. Visual inspections (Fig. 7(b)) of the films were also in good agreement with the UV-Vis spectroscopy finding, indicating that the compatibilizer has a positive effect on the transparency of the blended films.

Moisture barrier properties. High barrier properties are among the most important requirements when considering material for packaging applications, as goods need to be protected against moisture and gases. Water vapor permeability (WVP) test for the TPS/PLA blends with the presence of the *ex situ* compatibilizer St-PLA were carried out to evaluate the permeation of water vapor as a result of the compatibilization. As anticipated, the WVP of the TPS/PLA blends all fall between the permeability values of neat TPS and PLA. Comparing the neat TPS film with the TPS/PLA blend without a compatibilizer, the WVP values improved from 12.81 to $5.9 \times 10^{-13} \text{ kg m s}^{-1} \text{ m}^{-2} \text{ Pa}^{-1}$, which represents a 42.9% reduction (Fig. 8(a)). Thus, the introduction of PLA to the blend has helped improve the moisture barrier properties of neat TPS film, which is highly sensitive to moisture and water attack due to its inherent hydrophilicity.^{40,41}

It was also anticipated that the addition of St-PLA compatibilizer to the TPS/PLA blend would improve the overall moisture barrier properties of the films due to finer dispersion of PLA phase in the TPS matrices, as indicated from the results obtained from SEM and AFM analysis (Fig. S2, ESI†). However, contrary to expectation, the incremental addition of compatibilizer St-PLA in the blend formulation gradually increases the WVP of the TPS/PLA blend film, indicating that St-PLA diminished the water barrier properties of the blend films. The reason for this counterintuitive observation could be related to the reduction in the crystalline structures. A study conducted by Duan and Thomas investigated the correlation between the rate of crystallization of PLA and the solubility factor that contributes to the water vapour transmission rate (WVTR).⁴² The authors have found out that the crystalline spherulite can be treated as “impermeable” by water vapor, and that the solubility coefficient of the semi-crystalline PLA is the same as the solubility coefficient of the amorphous phase of PLA. Based on their investigations, it was concluded that the WVP is directly related to the crystalline spherulite structures. In this study, the results from POM and DSC suggested that the crystallinity of the TPS/PLA blend was reduced with the

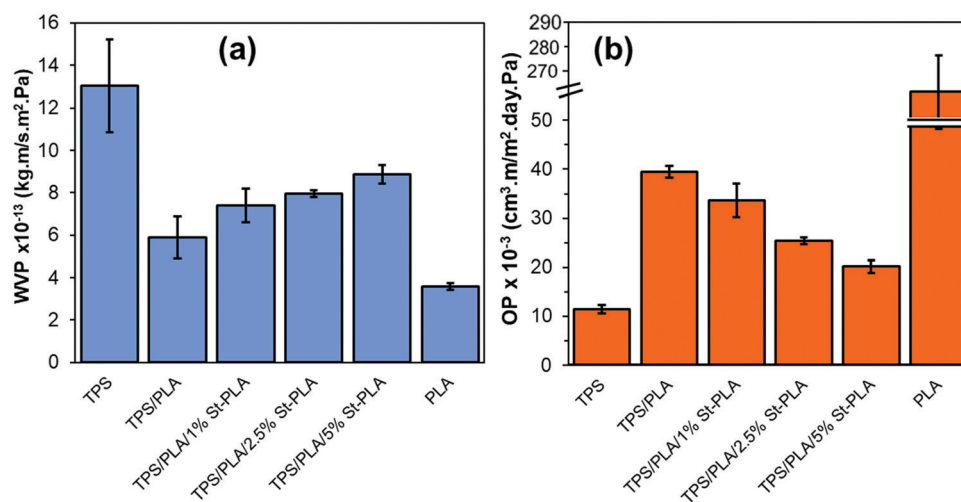


Fig. 8 Comparison of (a) WVP values, and (b) OP values of neat TPS, PLA, non-compatibilized, and compatibilized TPS/PLA blends.

addition of St-PLA compatibilizer, which explained the increasing WVP as shown in Fig. 8(a).

Oxygen barrier properties. The oxygen barrier properties of the TPS/PLA blend films were evaluated by employing the oxygen permeability (OP) test. Notably, the neat PLA films, known to provide poor oxygen barrier properties due to its hydrophobicity, displayed an extremely high OP of $221.55 \pm 20.65 \times 10^{-3} \text{ cm}^3 \text{ m m}^{-2} \text{ day}^{-1} \text{ Pa}^{-1}$. On the other hand, TPS films exhibited excellent oxygen permeability, with an OP value of $11.41 \times 10^{-3} \text{ cm}^3 \text{ m m}^{-2} \text{ day}^{-1} \text{ Pa}^{-1}$, as shown in Fig. 8(b). The lower oxygen permeation (high barrier) properties of the TPS can be explained by its inherent hydrophilicity in conjunction with its crystalline structure accrued from intermolecular and intramolecular bonding that inhibit the free mobility of oxygen molecules. These low permeability values were also observed in all the blend formulations which contain TPS as their ingredients. Incorporating the St-PLA compatibilizer promoted the enhancement in barrier properties with a linear relationship. At 5 wt% compatibilizer loading, the oxygen barrier has improved by 96% compared to TPS/PLA blend without a compatibilizer, and about 1052% compared to the neat PLA film. The improved oxygen barrier properties, stemming from the addition of St-PLA, attributed to the enhanced compatibility between the two polymer phases in the blends, which effectively decrease the free volume within the blend and reduce the diffusive mobility of the oxygen permeant. A similar trend was observed in a 1:1 ratio PLA/TPS (blend compatibilized by oligo lactic acid-PLA).³⁵ The researchers reported a reduction in the OP values by up to 64% compared to neat PLA and up to 20% compared to the same blend without compatibilizers.

Furthermore, the oxygen permeability experimental results were compared with the values predicted by the Maxwell and Bruggeman equations, which are among the most commonly used predictive models to determine the effective permeability of particulate filled continuous phase system.^{43–45} Maxwell's model assumes that the dispersed polymer phase consists of spherical solids that are homogeneous in the continuous phase, while Bruggeman equation utilized the concept of effective medium theory and is more applicable in randomly distributed dispersed phase systems. Therefore, the theoretical permeability (P) of TPS/PLA blend can be computed using either of Maxwell (eqn (5)) and Bruggeman (eqn (6)):

$$P = P_c \left[\frac{P_d + 2P_c - 2\Phi_d(P_c - P_d)}{P_d + 2P_c + \Phi_d(P_c - P_d)} \right] \quad (5)$$

$$\left(\frac{P}{P_c} - \frac{P_d}{P_c} \right) \left(\frac{P}{P_c} \right)^{-1/3} = (1 - \Phi_d) \left(1 - \frac{P_d}{P_c} \right) \quad (6)$$

where Φ_d is the fractional volumes of the dispersed polymer (PLA) phases, which was determined to be 0.357 based on the weight composition and the density of each component in the blend. P_c and P_d are the permeability of the continuous (TPS) and dispersed (PLA) phases, respectively. In this study, a P_c and P_d value of 10.82 and $265.01 \times 10^{-3} \text{ cm}^3 \text{ m m}^{-2} \text{ day}^{-1} \text{ Pa}^{-1}$, respectively were used. The oxygen permeability of the

uncompatibilized TPS/PLA blend based on Maxwell model (eqn (5)) was $27.13 \times 10^{-3} \text{ cm}^3 \text{ m m}^{-2} \text{ day}^{-1} \text{ Pa}^{-1}$, and from Bruggeman (eqn (6)) were $32.92 \times 10^{-3} \text{ cm}^3 \text{ m m}^{-2} \text{ day}^{-1} \text{ Pa}^{-1}$. The results from the Bruggeman model were in close agreement with the experimental value of $39.44 \times 10^{-3} \text{ cm}^3 \text{ m m}^{-2} \text{ day}^{-1} \text{ Pa}^{-1}$. On the other hand, the OP obtained from the Maxwell model is closer to the values obtained for the compatibilized blend at 2.5 and 5 wt% St-PLA with 25.36 and $20.13 \times 10^{-3} \text{ cm}^3 \text{ m m}^{-2} \text{ day}^{-1} \text{ Pa}^{-1}$, respectively. Though Maxwell's model tends to overestimate the permeability values at higher dispersed volume fractions, it is still a good indicator that the PLA phased is well dispersed within the TPS matrices in the presence of a St-PLA compatibilizer, as the model assumes even distribution of the dispersed phase. Overall, the enhancement in the interfacial compatibility of TPS and PLA promoted by the St-PLA compatibilizer has helped improve the oxygen barrier properties of the immiscible TPS/PLA blend. This is a commercially relevant observation for the food, biomedical, and pharmaceutical packaging applications, in which there is a dire need to prevent oxygen permeation as it causes oxidation of packaged products and consequently shorter shelf-life.

Mechanical properties. Evaluation of the mechanical properties provides essential information on the interfacial compatibility between TPS and PLA phases in the blend. The tensile properties of the investigated samples are presented in Fig. 9(a)–(d). Overall, the TPS film exhibited inferior tensile properties with tensile strength and modulus of 2.33 MPa and 37.85 MPa, respectively. On the contrary, the TPS/PLA film exhibited a significant boost in the tensile strength and modulus with a tensile strength of 5.83 MPa ($\sim 150\%$ increase) and a modulus of 472.82 MPa ($\sim 1.150\%$ improvement) due to the presence of PLA, respectively. However, the elongation at break of the ductile TPS was severely reduced as it was blended with the stiff PLA, and the elongation of the blend was even lower than that of the brittle PLA (Fig. 9(c) and Table S2, ESI†). Other studies, such as Teixeira *et al.*, also observed up to 30% ductility reduction for their thermoplastic cassava starch/PLA (20/80) blend compared to PLA.⁴⁶ This phenomenon was attributed to the poor interfacial interaction in the TPS/PLA blend, which results in rough morphology and increased brittleness, as noted in the SEM (Fig. 4).

It was evident that the addition of the St-PLA compatibilizer had both reinforcing and plasticization effect on the TPS/PLA blend. At a loading level of only 1 wt%, the compatibilization effect was not observed as the amount was not significant enough to make a difference in mechanical properties. With the use of 5 wt% St-PLA compatibilizer, the tensile strength of the uncompatibilized TPS/PLA blend increased from 5.83 to 10.21 MPa, which was a 75% improvement. Moreover, the ductility of the blend has also considerably improved with the gradual increase in the St-PLA concentration, which indicate an enhancement in the toughness of the compatibilized blend. At the highest loading of St-PLA (5 wt%), the elongation at break of the binary blends increased from 1.65 to 4.25% ($\sim 160\%$ increase), showing significant improvement in the film's flexibility. This augmentation in the film flexibility showed a great



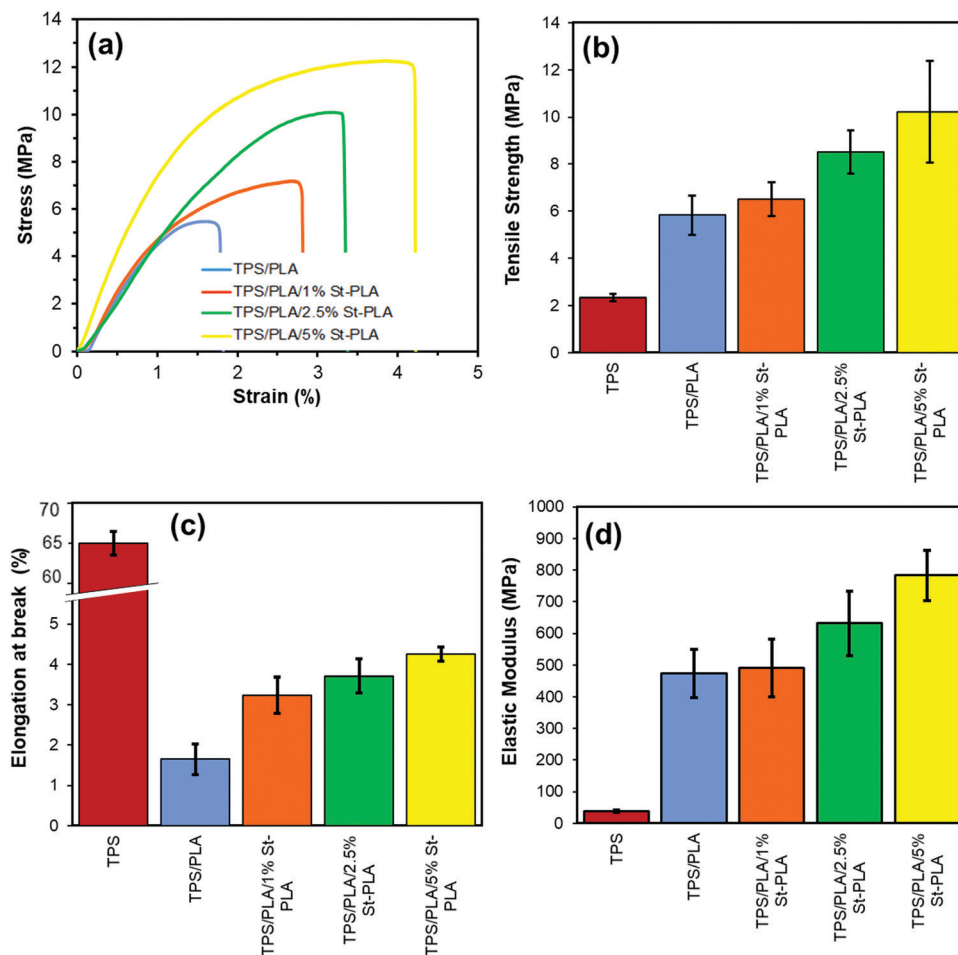


Fig. 9 Tensile properties of TPS/PLA blended films with increasing concentration of compatibilizer St-PLA, showing the (a) representative stress-strain curve of various TPS/PLA blends (b) Tensile strength, (c) elongation at break, and (d) elastic modulus.

potential to mitigate the brittleness caused by poor interfacial compatibility of the immiscible TPS and PLA materials. The elastic modulus, similar to tensile strength and flexibility, showed a tremendous improvement using the St-PLA compatibilizer. For instance, the use of 5 wt% St-PLA led to a 66% increase in the modulus compared to the uncompatibilized samples. Overall, extensive tensile property improvements were noted using the St-PLA *ex situ* compatibilizer, owing to the blends enhanced interfacial adhesion and phase dispersion.

4. Conclusion

Starch-graft-PLA (St-PLA) copolymer was successfully synthesized *via* the ROP reaction of lactide to deposit PLA oligomer on the starch backbone as confirmed *via* FTIR, NMR, DSC, and WCA evaluations. The use of optimal concentration of the St-PLA as a compatibilizer of TPS/PLA blend displayed outstanding compatibility and miscibility of the phases through interfacial bridging between the TPS and PLA chains. Consequently, the fabricated TPS/PLA films exhibited enhanced tensile properties in conjunction with superior oxygen barrier properties owing to the excellent distribution of PLA phases in

the TPS matrices. Nevertheless, it was also noted that the bridging between TPS and PLA phases through the *ex situ* compatibilization reduced the crystalline morphology of PLA structures. While such crystal spherulite reduction of the PLA promoted increased flexibility and transparency of the fabricated films, it also caused an undesirable moisture barrier reduction. Overall, this research conclusively demonstrated the great potential of using St-PLA co-polymers as a sustainable compatibilizing agent of TPS/PLA blends. The studied compatibilized blend is expected to be compostable with substantial application potential for food, pharmaceutical, and biomedical packaging, owing to its outstanding oxygen barrier and other physicochemical properties.

Author contributions

Binh M. Trinh: methodology, writing – original draft, writing – review & editing, results analysis, and conceptualization. Debela T. Tadele: writing – original draft, writing – review & editing, and results analysis. Tizazu H. Mekonnen: conceptualization, writing – review & editing, resources, and supervision.



Conflicts of interest

The authors declare that they have no known competing financial interests or personal relationships that could have appeared to influence the work reported in this paper.

Acknowledgements

The financial support of NSERC and Canada Foundation for Innovation is greatly appreciated. We would also like to thank Dr Arvind Gupta for the technical support he offered on this work.

References

- 1 R. Muthuraj and T. Mekonnen, Recent progress in carbon dioxide (CO₂) as feedstock for sustainable materials development: Co-polymers and polymer blends, *Polymer*, 2018, **145**, 348–373, DOI: [10.1016/j.polymer.2018.04.078](#).
- 2 O. H. P. Gunawardene, C. Gunathilake, S. M. Amaraweera, N. M. L. Fernando, D. B. Wanninayaka, A. Manamperi, A. K. Kulatunga, S. M. Rajapaksha, R. S. Dassanayake, C. A. N. Fernando and A. Manipura, Compatibilization of starch/synthetic biodegradable polymer blends for packaging applications: A review, *J. Compos. Sci.*, 2021, **5**, 300, DOI: [10.3390/JCS5110300](#).
- 3 A. K. Mohanty, M. Misra and G. Hinrichsen, Biofibres, biodegradable polymers and biocomposites: An overview, *Macromol. Mater. Eng.*, 2000, **276**–277, 1–24, DOI: [10.1002/\(SICI\)1439-2054\(20000301\)276:1<1::AID-MAME1>3.0.CO;2-W](#).
- 4 T. Mekonnen, P. Mussone, H. Khalil and D. Bressler, Progress in bio-based plastics and plasticizing modifications, *J. Mater. Chem. A*, 2013, **1**, 13379–13398, DOI: [10.1039/c3ta12555f](#).
- 5 T. Gurunathan, S. Mohanty and S. K. Nayak, A review of the recent developments in biocomposites based on natural fibres and their application perspectives, *Composites, Part A*, 2015, **77**, 1–25, DOI: [10.1016/j.compositesa.2015.06.007](#).
- 6 B. M. Trinh, C. C. Chang and T. H. Mekonnen, Facile fabrication of thermoplastic starch/poly(lactic acid) multilayer films with superior gas and moisture barrier properties, *Polymer*, 2021, **223**, 123679, DOI: [10.1016/J.POLYMER.2021.123679](#).
- 7 B. Palai, M. Biswal, S. Mohanty and S. K. Nayak, *In situ* reactive compatibilization of polylactic acid (PLA) and thermoplastic starch (TPS) blends; synthesis and evaluation of extrusion blown films thereof, *Ind. Crops Prod.*, 2019, **141**, 111748, DOI: [10.1016/J.INDCROP.2019.111748](#).
- 8 S. Detyothin, A. Kathuria, W. Jaruwattanayon, S. E. M. Selke and R. Auras, Poly(Lactic Acid) Blends, *Poly(Lactic Acid)*, John Wiley & Sons, Inc., Hoboken, NJ, USA, 2010, pp.227–271, DOI: [10.1002/9780470649848.ch16](#).
- 9 S. K. Ghosh, T. K. Das, S. Ghosh, S. Remanan, K. Nath, P. Das and N. C. Das, Selective distribution of conductive carbonaceous inclusion in thermoplastic elastomer: A wet chemical approach of promoting dual percolation and inhibiting radiation pollution in X-band, *Compos. Sci. Technol.*, 2021, **210**, 108800, DOI: [10.1016/J.COMPOSITECH.2021.108800](#).
- 10 S. K. Ghosh, T. K. Das, S. Ganguly, K. Nath, S. Paul, D. Ganguly and N. C. Das, Silane functionalization of sodium montmorillonite and halloysite (HNT) nanoclays by 'grafting to' method to improve physico-mechanical and barrier properties of LLDPE/clay nanocomposites, *Polym. Bull.*, 2022, **2022**, 1–29, DOI: [10.1007/S00289-022-04281-4](#).
- 11 C. C. Chang, B. M. Trinh and T. H. Mekonnen, Robust multiphase and multilayer starch/polymer (TPS/PBAT) film with simultaneous oxygen/moisture barrier properties, *J. Colloid Interface Sci.*, 2021, **593**, 290–303, DOI: [10.1016/J.JCIS.2021.03.010](#).
- 12 E. Ojogbo, E. O. Ogunsona and T. H. Mekonnen, Chemical and physical modifications of starch for renewable polymeric materials, *Mater. Today Sustain.*, 2020, **7**–8, 100028, DOI: [10.1016/j.mtsust.2019.100028](#).
- 13 T. Mekonnen, P. Mussone, H. Khalil and D. Bressler, Progress in bio-based plastics and plasticizing modifications, *J. Mater. Chem. A*, 2013, **1**, 13379–13398, DOI: [10.1039/C3TA12555F](#).
- 14 D. Jubinville, B. P. Chang, J. M. Pin, A. K. Mohanty and M. Misra, Synergistic thermo-oxidative maleation of PA11 as compatibilization strategy for PA6 and PBT blend, *Polymer*, 2019, **179**, 121594, DOI: [10.1016/J.POLYMER.2019.121594](#).
- 15 R. Muthuraj, M. Misra and A. K. Mohanty, Biodegradable compatibilized polymer blends for packaging applications: A literature review, *J. Appl. Polym. Sci.*, 2018, **135**, 45726, DOI: [10.1002/APP.45726](#).
- 16 D. Jubinville, E. Esmizadeh, S. Saikrishnan, C. Tzoganakis and T. Mekonnen, A comprehensive review of global production and recycling methods of polyolefin (PO) based products and their post-recycling applications, *Sustainable Mater. Technol.*, 2020, **25**, e00188, DOI: [10.1016/J.SUSMAT.2020.E00188](#).
- 17 M. A. Huneault and H. Li, Morphology and properties of compatibilized polylactide/thermoplastic starch blends, *Polymer*, 2007, **48**, 270–280, DOI: [10.1016/J.POLYMER.2006.11.023](#).
- 18 J. Wootthikanokkhan, P. Kasemwananimit, N. Sombatsompop, A. Kositchaiyong and S. Isarankura, na Ayutthaya, N. Kaab- buathong, Preparation of modified starch-grafted poly(lactic acid) and a study on compatibilizing efficacy of the copolymers in poly(lactic acid)/thermoplastic starch blends, *J. Appl. Polym. Sci.*, 2012, **126**, E389–E396, DOI: [10.1002/app.36896](#).
- 19 R. Turco, R. Ortega-Toro, R. Tesser, S. Mallardo, S. Collazo-Bigliardi, A. C. Boix, M. Malinconico, M. Rippa, M. Di Serio and G. Santagata, Poly(lactic acid)/thermoplastic starch films: Effect of cardoon seed epoxidized oil on their chemico-physical, mechanical, and barrier properties, *Coatings*, 2019, **9**, 1–20, DOI: [10.3390/coatings9090574](#).
- 20 Q. Shi, C. Chen, L. Gao, L. Jiao, H. Xu and W. Guo, Physical and degradation properties of binary or ternary blends composed of poly(lactic acid), thermoplastic starch and GMA grafted POE, *Polym. Degrad. Stab.*, 2011, **96**, 175–182, DOI: [10.1016/J.POLYMDEGRADSTAB.2010.10.002](#).



- 21 L. Chen, X. Qiu, M. Deng, Z. Hong, R. Luo, X. Chen and X. Jing, The starch grafted poly(l-lactide) and the physical properties of its blending composites, *Polymer*, 2005, **46**, 5723–5729, DOI: [10.1016/j.polymer.2005.05.053](https://doi.org/10.1016/j.polymer.2005.05.053).
- 22 H. Eslami, C. Tzoganakis and T. H. Mekonnen, Constructing pristine and modified cellulose nanocrystals based cured polychloroprene nanocomposite films for dipped goods application, *Composites Part C: Open Access*, 2020, **1**, 100009, DOI: [10.1016/J.JCOMC.2020.100009](https://doi.org/10.1016/J.JCOMC.2020.100009).
- 23 H. Eslami, T. Costas and T. H. Mekonnen, Surface graft polymerization of lactic acid from the surface of cellulose nanocrystals and applications in chloroprene rubber film composites, *Cellulose*, 2020, **27**, 5267–5284, DOI: [10.1007/s10570-020-03167-w](https://doi.org/10.1007/s10570-020-03167-w).
- 24 R. Lipsa, N. Tudorachi, C. Vasile, A. Chiriac and A. Grigoras, Novel environmentally friendly copolymers carboxymethyl starch grafted poly(lactic acid), *J. Polym. Environ.*, 2013, **21**, 461–471, DOI: [10.1007/S10924-012-0470-1/FIGURES/10](https://doi.org/10.1007/S10924-012-0470-1/FIGURES/10).
- 25 S. Jia, D. Yu, Y. Zhu, Z. Wang, L. Chen and L. Fu, Morphology, crystallization and thermal behaviors of PLA-based composites: Wonderful effects of hybrid GO/PEG *via* dynamic impregnating, *Polymers*, 2017, **9**(10), 528, DOI: [10.3390/polym9100528](https://doi.org/10.3390/polym9100528).
- 26 E. Ojogbo, R. Blanchard and T. Mekonnen, Hydrophobic and melt processable starch-laurate esters: Synthesis, structure-property correlations, *J. Polym. Sci., Part A: Polym. Chem.*, 2018, **56**, 2611–2622, DOI: [10.1002/pola.29237](https://doi.org/10.1002/pola.29237).
- 27 B. M. Trinh and T. Mekonnen, Hydrophobic esterification of cellulose nanocrystals for epoxy reinforcement, *Polymer*, 2018, **155**, 64–74, DOI: [10.1016/j.polymer.2018.08.076](https://doi.org/10.1016/j.polymer.2018.08.076).
- 28 S. S. Zamir, M. R. Frouzanmehr, M. Nagalakshmaiah, A. Ajji, M. Robert and S. Elkoun, Chemical compatibility of lactic acid-grafted starch nanocrystals (SNCs) with polylactic acid (PLA), *Polym. Bull.*, 2019, **76**, 3481–3499, DOI: [10.1007/S00289-018-2548-Y](https://doi.org/10.1007/S00289-018-2548-Y).
- 29 J. Liu, X. Wang, R. Bai, N. Zhang, J. Kan and C. Jin, Synthesis, characterization, and antioxidant activity of caffeic-acid-grafted corn starch, *Starch – Stärke.*, 2018, **70**, 1700141, DOI: [10.1002/star.201700141](https://doi.org/10.1002/star.201700141).
- 30 E. Ojogbo, R. Blanchard and T. Mekonnen, Hydrophobic and melt processable starch-laurate graft polymers: Synthesis, structure – property correlations, *J. Polym. Sci., Part A: Polym. Chem.*, 2018, **56**, 2611–2622, DOI: [10.1002/pola.29237](https://doi.org/10.1002/pola.29237).
- 31 E. Ojogbo, V. Ward and T. H. Mekonnen, Functionalized starch microparticles for contact-active antimicrobial polymer surfaces, *Carbohydr. Polym.*, 2020, **229**, 115422, DOI: [10.1016/j.carbpol.2019.115422](https://doi.org/10.1016/j.carbpol.2019.115422).
- 32 Y. Wen, F. Ye, J. Zhu and G. Zhao, Corn starch ferulates with antioxidant properties prepared by *N,N'*-carbonyldiimidazole-mediated grafting procedure, *Food Chem.*, 2016, **208**, 1–9, DOI: [10.1016/j.foodchem.2016.03.094](https://doi.org/10.1016/j.foodchem.2016.03.094).
- 33 K. Suganuma, T. Asakura, M. Oshimura, T. Hirano, K. Ute and H. N. Cheng, NMR analysis of poly(lactic acid) *via* statistical models, *Polymers*, 2019, **11**, 1–8, DOI: [10.3390/polym11040725](https://doi.org/10.3390/polym11040725).
- 34 B. M. Trinh, E. O. Ogunsona and T. H. Mekonnen, Thin-structured and compostable wood fiber-polymer biocomposites: Fabrication and performance evaluation, *Composites, Part A*, 2021, **140**, 106150, DOI: [10.1016/j.compositesa.2020.106150](https://doi.org/10.1016/j.compositesa.2020.106150).
- 35 N. Noivoil and R. Yoksan, Oligo(lactic acid)-grafted starch: A compatibilizer for poly(lactic acid)/thermoplastic starch blend, *Int. J. Biol. Macromol.*, 2020, **160**, 506–517, DOI: [10.1016/j.ijbiomac.2020.05.178](https://doi.org/10.1016/j.ijbiomac.2020.05.178).
- 36 C. Zhang, Y. Huang, C. Luo, L. Jiang and Y. Dan, Enhanced ductility of polylactide materials: Reactive blending with pre-hot sheared natural rubber, *J. Polym. Res.*, 2013, **20**(121), 1–9, DOI: [10.1007/S10965-013-0121-9](https://doi.org/10.1007/S10965-013-0121-9).
- 37 J. Shawe, R. Riesen, J. Widmann and M. Schubnell, Interpreting DSC curves Part 1: Dynamic measurements, 2000.
- 38 M. Esmaeili, G. Pircheraghi, R. Bagheri and V. Altstädt, Poly(lactic acid)/coplasticized thermoplastic starch blend: Effect of plasticizer migration on rheological and mechanical properties, *Polym. Adv. Technol.*, 2019, **30**, 839–851, DOI: [10.1002/PAT.4517](https://doi.org/10.1002/PAT.4517).
- 39 Y. Lin, E. Bilotti, C. W. M. Bastiaansen and T. Peijs, Transparent semi-crystalline polymeric materials and their nanocomposites: A review, *Polym. Eng. Sci.*, 2020, **60**, 2351–2376, DOI: [10.1002/PEN.25489](https://doi.org/10.1002/PEN.25489).
- 40 E. Ogunsona, E. Ojogbo and T. Mekonnen, Advanced material applications of starch and its derivatives, *Eur. Polym. J.*, 2018, **108**, 570–581, DOI: [10.1016/j.eurpolymj.2018.09.039](https://doi.org/10.1016/j.eurpolymj.2018.09.039).
- 41 E. Hablot, S. Dewasthale, Y. Zhao, Y. Zhiguan, X. Shi, D. Graiver and R. Narayan, Reactive extrusion of glycerylated starch and starch-polyester graft copolymers, *Eur. Polym. J.*, 2013, **49**, 873–881, DOI: [10.1016/j.eurpolymj.2012.12.005](https://doi.org/10.1016/j.eurpolymj.2012.12.005).
- 42 Z. Duan and N. L. Thomas, Water vapour permeability of poly(lactic acid): Crystallinity and the tortuous path model, *J. Appl. Phys.*, 2014, **115**, 064903, DOI: [10.1063/1.4865168](https://doi.org/10.1063/1.4865168).
- 43 E. E. Gonzo, M. L. Parentis and J. C. Gottifredi, Estimating models for predicting effective permeability of mixed matrix membranes, *J. Membr. Sci.*, 2006, **277**, 46–54, DOI: [10.1016/J.MEMSCI.2005.10.007](https://doi.org/10.1016/J.MEMSCI.2005.10.007).
- 44 A. Rybak, A. Rybak and P. Sysel, Modeling of gas permeation through mixed-matrix membranes using novel computer application MOT, *Appl. Sci.*, 2018, **8**, 1–20, DOI: [10.3390/app8071166](https://doi.org/10.3390/app8071166).
- 45 J. H. Petropoulos, A comparative study of approaches applied to the permeability of binary composite polymeric materials, *J. Polym. Sci., Polym. Phys. Ed.*, 1985, **23**, 1309–1324, DOI: [10.1002/POL.1985.180230703](https://doi.org/10.1002/POL.1985.180230703).
- 46 E. de, M. Teixeira, A. A. S. Curvelo, A. C. Corrêa, J. M. Marconcini, G. M. Glenn and L. H. C. Mattoso, Properties of thermoplastic starch from cassava bagasse and cassava starch and their blends with poly(lactic acid), *Ind. Crops Prod.*, 2012, **37**, 61–68, DOI: [10.1016/J.INDCROP.2011.11.036](https://doi.org/10.1016/J.INDCROP.2011.11.036).

